Investigations on Transient Temperature Distribution and Distortion in Shielded Metal Arc Welding of SA 516 Gr. 70 Steel

ORCID: Kalpeshkumar M. Sojitriya: https://orcid.org/0009-0005-3369-6897
ORCID: V. D. Kalyankar: https://orcid.org/0000-0002-7141-3705
ORCID: K. V. Champaneria: https://orcid.org/0009-0006-0828-3676
ORCID: G. P. Chudasama: https://orcid.org/0000-0002-9593-664X

DOI : 10.22486/iwj.v57i1.223728

Kalpeshkumar M. Sojitriya[1,a], V. D. Kalyankar[2,b], K. V. Champaneria[2,c], G. P. Chudasama[2,d]
[1]ISGEC Hitachi Zosen Limited, Dahej – 392130, Gujarat, India
[2]Advanced Welding Laboratory, Department of Mechanical Engineering
S. V. National Institute of Technology, Surat – 395007, Gujarat, India
[a]kalpeshsojitriya@gmail.com, [b]vivekkalyankar@yahoo.co.in
[c]karanchampaneria25@gmail.com, [d]gautamchudasama@gmail.com

Abstract

Efforts are made in this article to investigate the thermal and mechanical phenomena by presenting a coupled thermal and structural analysis of SA516 Grade-70 steel. This material has wide applicability in the fabrication of pressure vessels, boilers, etc., due to its excellent weldability and formability. An actual ongoing problem from a reputed industry, related to distortion during the shielded metal arc welding process, is considered and experiments are carried out on the chosen steel. Results are evaluated employing a two-step methodology, involving simulation. The first step encompasses thermal analysis, providing insights into transient temperature distribution, while the subsequent mechanical analysis offers data on residual stresses and distortion. In the case of heat input, a volumetric heat source with double ellipsoidal heat distribution is used whereas a plasticity material model with rate-independent bilinear kinematic hardening is adopted for the structural analysis. Additionally, temperature-dependent material properties are factored into both scenarios. The data derived from numerical analysis align closely with experimental findings, presenting valuable insights for fabricating industries.

Keywords : SMAW process, Simulation, Thermal analysis, Structural analysis, Goldak's heat source, Welding distortion, SA516 Grade-70 steel.

1.0 INTRODUCTION

In the welding process, there's typically an uneven temperature distribution, resulting in thermal stresses and distortion, which heavily depends on the material properties and the size/shape of the product. The residual stresses in welds can lead to issues like fractures due to tensile thermal stresses or a reduction in structural strength due to compressive thermal stresses. Therefore, it is best practice for a weld joint designer to predict the thermal stresses and distortion likely to develop in the material and take necessary actions accordingly. Due to the complexity of the physical phenomena involved in welding, simple mathematical solutions cannot address the practical welding processes. It is very difficult to obtain complete contours of residual stresses and distortion in a welded structure by experiment. So, computational simulation is crucial for analysing welded structures, although it is complex to model and takes more computational time.

In the literature, attempts were made by several researchers to model welding phenomena in which Lindgren [1] provided an overview ranging from heat generation and weld pool aspects to thermal stress and deformations of welded structures. Attarha and Sattari [2] carried out a thermal analysis using a double ellipsoidal heat source model using ABAQUS. Panwala et al. [3] explored how weld geometry influences transient temperature distributions. Some of the researchers also reported an approach of 2D surface heat source with Gaussian heat distributions for carrying out different thermal analysis [4-6].

Goldak et al. [7] developed a volumetric heat source model. Front and rear half volumetric heat sources were subsequently reported [8-10] to define accurate weld pool geometry. Barroso et al. [11] explored several simple hypotheses used in welding simulation for time reduction and performed influences of those hypotheses with experimental validation. Jia et al. [12] developed a new method to calculate heat source parameters during welding simulation whereas, Bhatti et al. [13] studied the impact of thermo-mechanical characteristics of various steels on residual stress and angular distortion.

Yadav et al. [14] used the heat source model with oval shape for the submerged arc welding (SAW) to predict the transient temperature distribution along with other relevant aspects. An analytical solution was derived by Ghosh et al. [15] for the central conicoidal shape by using moving heat source with Gaussian distribution. A critical assessment of temperature distribution is carried out by Negi and Chattopadhyaya [16] by attempting a temperature distribution model during the SAW process using the finite element (FE) modelling technique.

Chang and Teng [17] performed thermal elastic-plastic analysis of butt-welded joints by employing FE techniques to evaluate residual stresses. Deng and Murakawa [18] utilized the FE method for simulating distortion of a butt joint of low-carbon steel. Zhu and Chao [19] carried out 3D non-linear thermo-mechanical analyses through process simulation. Teng et al. [20] investigated how the process parameters and constraints influenced the weld residual stresses. Li and Wang [21] analysed temperature and stress distributions during in-service welding of pipeline steel, highlighting the significant influence of flowing water on residual stress. Apart from this, a few researchers also investigated the residual stresses and distortion on various other welding processes using the FE analysis approach [22-24]. Further, the use of such simulation and numerical analysis of the process is effectively applied by the researchers to other fields of engineering such as Wei et al. [25] used a simulation approach to study the heat transfer mechanism of the composite insulation coating, Kalyankar and Pujari [26] used the simulation approach to design the broach tool geometry.

From the literature, it is observed that a widely used material in pressure vessels, SA516 Grade-70 steel, was rarely considered in earlier works to study the thermo-mechanical analysis, particularly for the shielded metal arc welding (SMAW) process, which is still finding large applications to weld various ranges of products due to its flexibility. This material finds considerable application in fabricating pressure vessels and similar products because of its excellent formability and weldability. It offers higher strength at lower and higher temperature range and also possesses excellent notch toughness which makes it a better choice material for pressure vessels and industrial boilers. However, poor quality welding along with undesirable properties may result, if proper precaution is not taken for temperature distribution over the material during the welding operation, especially with SMAW which is a more suitable and widely used process for such types of applications. Hence, an actual ongoing problem of a reputed pressure vessel fabricating industry is considered here and attempts are made to present a coupled thermal and structural analysis of the SMAW process to access temperature distribution, residual stress and distortion of the chosen material. Welders and engineers were facing continuous problems of distortion despite taking all necessary precautions. Hence, a simulation model is developed for the product under consideration and it is simulated with different realistic conditions and the simulated results are validated through experiments. The results obtained are very encouraging to the industry personnel and the same are described in the subsequent sections.

2.0 NUMERICAL MODELLING

Welding comprises intricate interactions among diverse physical and metallurgical phenomena [8]. The FE analysis of welding is demanding and time-intensive due to the involvement of multiple factors such as material property, non-linearity, moving heat sources, intricate boundary conditions, and phase transformation effects. Hence, certain assumptions are made in this work that include consideration of the half geometry due to symmetry effects, weld material and the base material to be the same, and phase transformation effects are neglected.

2.1. Modelling approach

The thermo-mechanical model of a welding process consists of a thermal model with a volumetric heat source and a mechanical model with input from temperature distributions. By developing a user subroutine in ANSYS Parametric Design Language (APDL), a 3D numerical simulation of the SMAW process is carried out to predict transient temperature distribution, residual stress and distortion. Experiments are carried out on sample plates as shown in **Fig. 1**, each of size (100x50x4) mm with a single V groove joint. In numerical modelling, same welding conditions are considered as that used during the actual experiments.

The SOLID 70 element type, a linear 8 node brick element with one degree of freedom (each node temperature), is employed for 3D thermal analysis due to its capability for three-dimensional thermal conduction. This element is also applicable to a 3D steady state or transient thermal analysis. The element type should be changed to SOLID185 to conduct structural analysis. This element is a linear 8 node brick element with three degrees of freedom at each node, allowing translations in all the three directions. The total number of 8-node brick elements used for the numerical model in the present work is 9600.

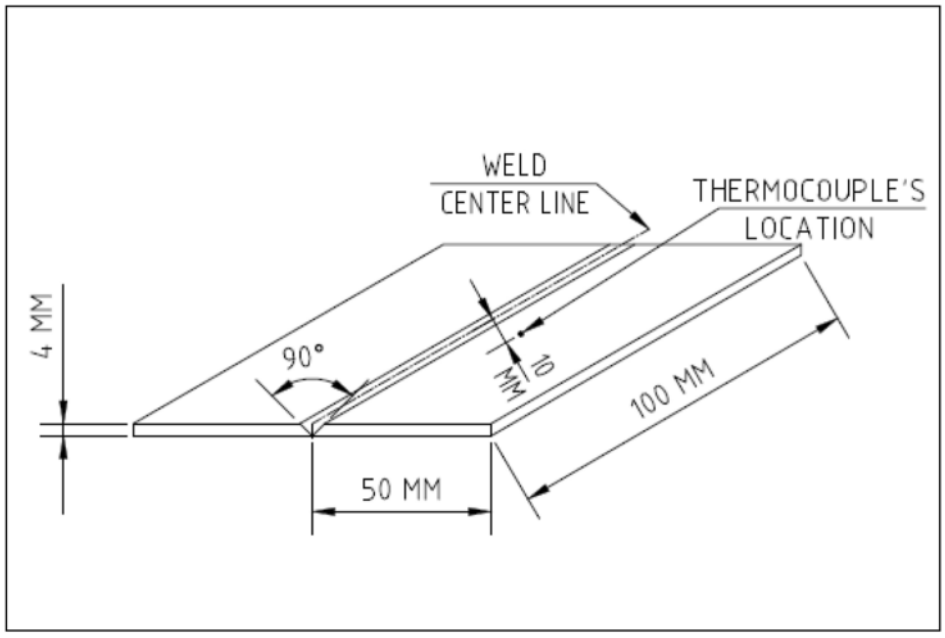

Fig. 1 : Geometry of test specimen

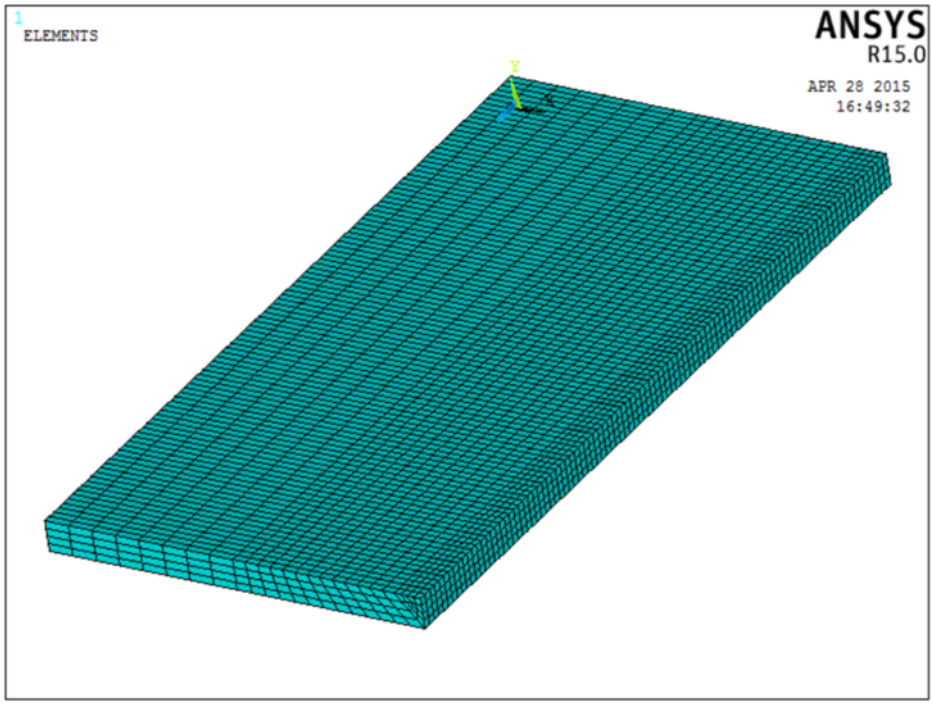

Fig. 2 : Image of adopted mesh for analysis

A finer mesh is utilized in the fusion zone and heat affected zone (HAZ) to enhance the precision of the heat source model. Subsequently, the meshing becomes coarser with increasing distance from the weld bead as shown in **Fig. 2**. Further, the thickness and width of the weld bead are divided into four numbers of elements. A non-linear geometrical phenomenon is incorporated in ANSYS to capture non-linear geometric behaviours and the Newton-Raphson option is used to solve non-linear equations analysis.

2.2. Thermal model

Accurate thermal analysis with meticulous attention to boundary conditions is crucial to derive realistic temperature profiles [27]. In welding processes, heat conduction prevails as the primary mode of heat transfer within the metal body, with heat convection playing a less impactful role in the weld's temperature distribution. The governing differential equation for heat conduction within a solid body enclosed by an arbitrary surface is represented by equation (1) [17]:

$$\frac{\partial}{\partial x}\left(K_x \frac{\partial T}{\partial x}\right) + \frac{\partial}{\partial y}\left(K_y \frac{\partial T}{dy}\right) + \frac{\partial}{\partial z}\left(K_z \frac{dT}{dz}\right) + Q(x,y,z,t) = \rho C \frac{\partial T(x,y,z,t)}{\partial t} \quad \text{.....(1)}$$

General solution to this differential equation is derived by applying following set of boundary conditions as shown by equations (2) and (3) [17]:

Initial condition:

$$T(x,y,z,0) = T_0(x,y,z) \quad \text{.....(2)}$$

Boundary condition:

$$\left(K_x \frac{\partial T}{\partial x} N_x + K_y \frac{\partial T}{\partial y} N_y + K_z \frac{\partial T}{\partial z} N_z\right) + q_s + h_c(T - T_\infty) + h_r(T - T_r) = 0 \quad \text{..... 3}$$

The radiation heat transfer coefficient, hr, required is expressed as shown in equation (4) [17]:

$$h_r = \sigma \varepsilon F(T^2 + T_r^2)(T + T_r) \quad \text{..... 4}$$

The initial condition required in equation (2) is taken equal to the room temperature and combined convection and radiation effects from all free surfaces of the body is adopted as the boundary condition for thermal analysis.

2.3. Heat source model

The most widely accepted double ellipsoidal heat source model with Gaussian heat distribution proposed by Goldak et al. [7] is used to model heat generation in the arc welding process. This is widely used to define the correct shape of the weld pool with high accuracy. It consists of a front half formed by a quadrant of an ellipsoid and a rear half formed by a quadrant of another ellipsoid, illustrated in **Fig. 3**. Two different parts give energy distribution i.e. for the front part as shown by equation (5) and for the rear part as shown by equation (6) [7]:

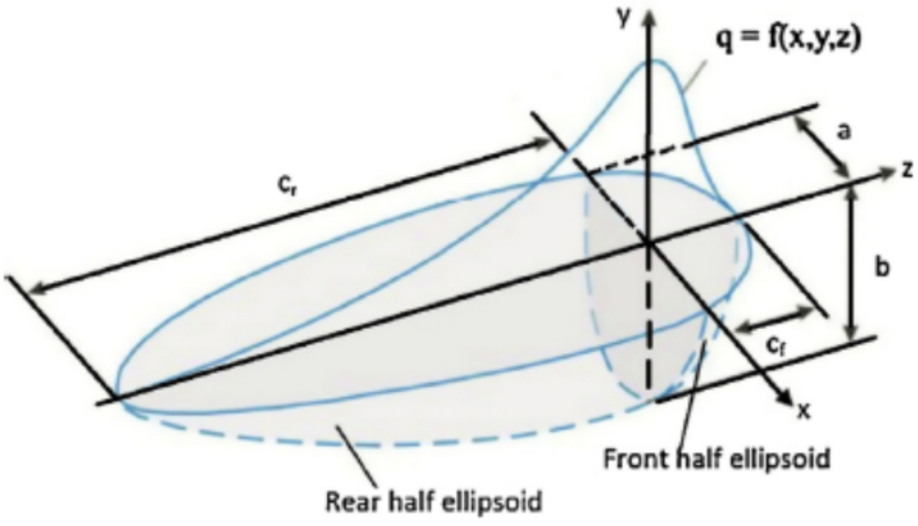

Fig. 3 : Goldak's double ellipsoidal heat source [12]

$$q(x,y,z,t) = \frac{6\sqrt{3}f_f Q}{abc_f\pi\sqrt{\pi}} e^{-\frac{3x^2}{a^2}} e^{-\frac{3y^2}{b^2}} e^{-\frac{3[z+v(\tau-t)]^2}{c_f^2}} \quad \ldots (5)$$

$$q(x,y,z,t) = \frac{6\sqrt{3}f_r Q}{abc_r\pi\sqrt{\pi}} e^{-\frac{3x^2}{a^2}} e^{-\frac{3y^2}{b^2}} e^{-\frac{3[z+v(\tau-t)]^2}{c_r^2}} \quad \ldots (6)$$

The available heat from an electric arc is calculated using the equation (7):

$$Q = \eta VI \quad \ldots . (7)$$

With several trials along with handbook recommendations, the parameter setting considered during the welding consists of welding voltage = 25 Volts, welding current = 90 Ampere, welding speed = 2.5 mm/sec, and arc efficiency = 0.65.

Fig. 4 : Cross section of weld bead after experiment

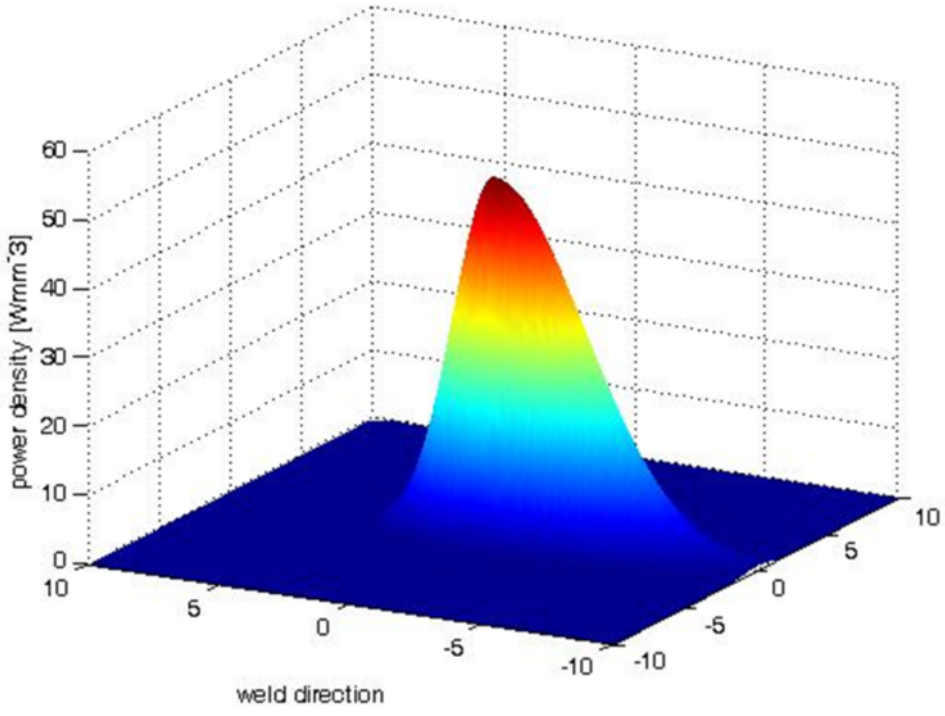

Fig. 5 : Heat flux distribution during welding

Table 1 : Goldak's heat source parameters obtained through measurements

Sr. No.	Parameters	Value
1	Width of heat source (mm), a	3.593
2	Depth of heat source (mm), b	2.267
3	Length of front ellipsoid (mm), c_f	3.593
4	Length of rear ellipsoid (mm), c_r	8.384
5	Fraction of heat in the front ellipsoidal, f_f	0.6
6	Fraction of heat in the rear ellipsoidal, f_r	1.4

Parameters a, b, c_f, and c_r correspond to the width, depth, front length, and rear length of the heat source, respectively which define the respective ellipsoids aligning with the dimensions of the molten zone. This model necessitates specifying fractions f_f and f_r representing the heat deposited in the front and rear quadrants, with the condition that $f_f + f_r = 2$. Accurate heat source parameters are obtained on the plate by performing three passes of weld bead, and their cross sections are measured after etching with nitric acid as shown in **Fig. 4**. The parameter "a" is evaluated by taking the average of half of the weld bead width, and parameter "b" is evaluated by taking the average of the weld bead height. Parameter "c_f" is taken as half of the weld bead width and "c_r" is calculated by equating equations (5) and (6) (at x=0, y=0 and z=0). Numerical values of Goldak's heat source parameters obtained through measurements are illustrated in **Table 1** and corresponding heat flux distribution is shown in **Fig. 5**.

2.4. Mechanical model

In the welding process, a thermal analysis must be followed by mechanical analysis to estimate residual stresses and distortion. FE model with the same geometry, as used in the thermal analysis, must be used for mechanical analysis too. The temperature history of each node obtained from thermal analysis is taken as structural load input for mechanical analysis. Suitable boundary conditions are determined empirically to restrict the rigid body motion of the plates. A mechanical model consists of two basic sets of equations namely equilibrium equations and constitutive equations. Equations (8) and (9) shown below correspond to equilibrium equations whereas equations (10) and (11) correspond to constitutive equations[17].

$$\sigma_{ij,j} + \rho b_i = 0 \quad \text{.... (8)}$$

$$\sigma_{ij} = \sigma_{ji} \quad \text{.... (9)}$$

$$[d\sigma] = [D^{ep}][d\varepsilon] - [C^{th}]dT \quad \text{.... (10)}$$

$$[D^{ep}] = [D^{e}] + [D^{p}] \quad \text{.... (11)}$$

The accumulated rate-dependent plasticity is neglected in this work; as high temperature occurs only for a short duration of time. Moreover, a material model with rate-independent plasticity, based on von Mises yield criterion, is used in this work.

Table 2 : Chemical composition of SA516 Grade-70 steel (weight%)

C	S	P	Si	Mn	Ni	Cr
0.202	0.001	0.009	0.298	1.190	0.009	0.106

2.5. Material details

The base plates utilized in this study are made of low carbon steel SA516 Grade-70. This material is extensively employed in various industries including pressure vessel fabrication, nuclear sectors, chemical plants, shipbuilding, and specialized pipe industries. A chemical analysis of chosen material is carried out using optical emission spectrometry and same is shown in **Table 2**.

The complete range of temperature-dependent material properties for SA516 Grade-70 steel is not available in the literature. Therefore, the material properties as reported by Karlsson and Josefson [28], having nearly the same chemical compositions, are considered in the numerical modelling, and the same is shown in **Fig. 6** and **Fig. 7**. Furthermore, the temperature-dependent heat transfer coefficient is taken from the work of Brown and Song [29], and Panwala et al.[3] also shows the similar type of material selection approach.

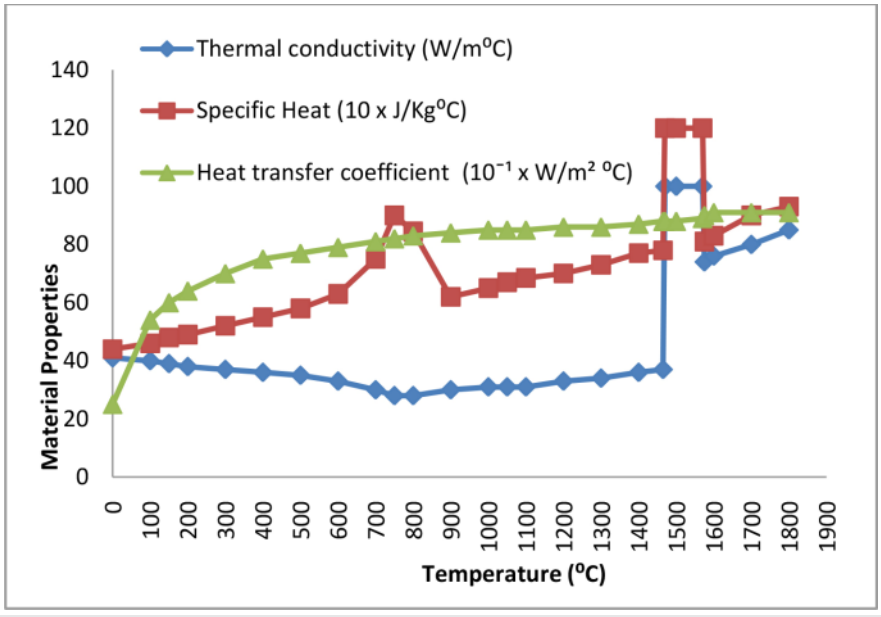

Fig. 6 : Temperature-dependant thermal properties of SA516 Grade-70 steel [28-29]

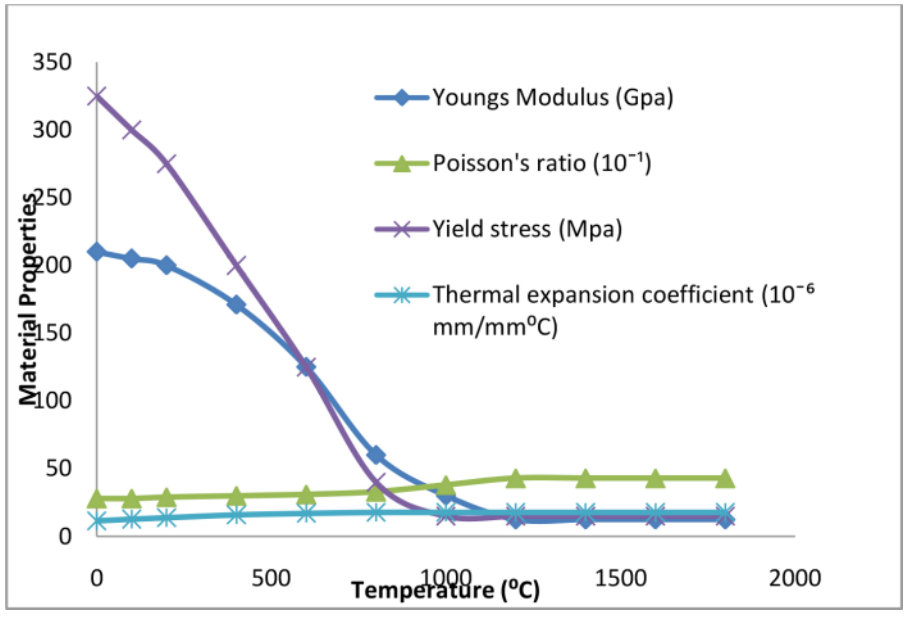

Fig. 7: Temperature-dependant mechanical properties of SA516 Grade-70 steel [28]

3.0 EXPERIMENTAL APPROACH

In this study, experiments were conducted to measure the temperature history at a defined point on the top surface using K-type thermocouples and distortion at the extreme edge of welded plates. Two steel plates of (100x50x4) mm size, with single V-groove (90°) between them, are welded using SMAW process is shown in **Fig. 8**. Welding electrode E7018 with 2.5 mm diameter is used which consists of low hydrogen potassium and iron powder covering. The temperature history is recorded at 10 mm away from the weld centre line by mounting K-type thermocouples at the chosen point. Continuous recording of temperature is done by attaching highly accurate and good quality thermocouples to the data recording device, and welding speed is determined by averaging the time taken for the welding. Mahapatra et al. [5] also supports the same type of approach. Deformation of welded plates is measured at mid-length of the plates, using a vernier calliper having least count of 0.02 mm with the method presented by Deng and Murakawa[18]. Results obtained through experiments are presented in the next section along with the analysis.

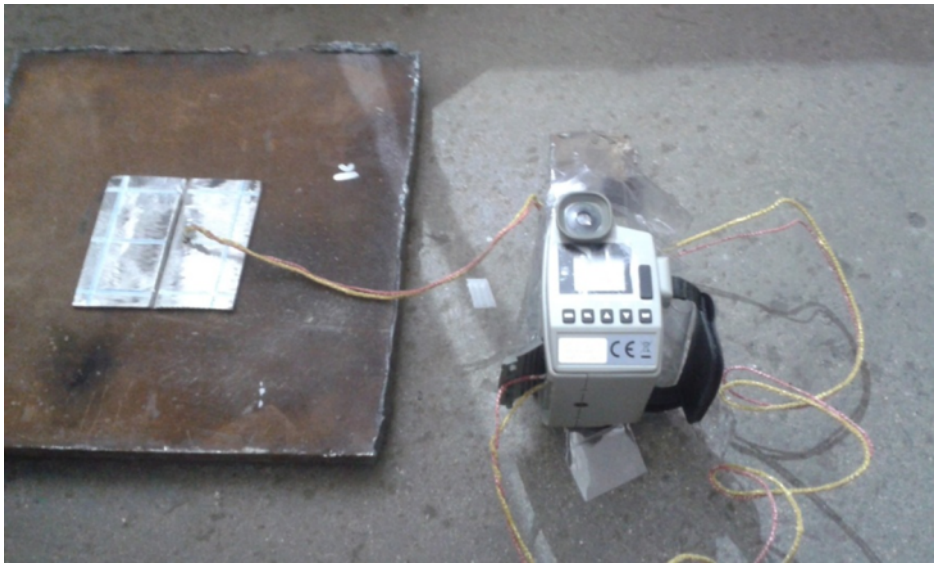

Fig. 8 : Experimental setup

4.0 RESULTS AND DISCUSSIONS

4.1 Result of thermal analysis

Thermal analysis of the welded joint is carried out in ANSYS until the steady state condition is reached. **Fig. 9(a)–(b)** shows recorded temperature distributions at different time intervals. The temperature in the fusion zone is found to be more than the melting temperature of the base material, and the centre of the heat source has shown the highest temperature. A steep temperature gradient is recorded ahead of the electrode and a significant temperature gradient behind the electrode shows cooling phenomena after achieving peak temperature.

Fig. 10 shows temperature distribution along the transverse direction (perpendicular to the weld centreline) at different time intervals. The transverse direction has shown a non-linear temperature gradient, and a high-temperature gradient occurs near the weld bead. Heat dissipation continues from the weld centreline to the edges of a base plate, through conduction phenomena, till achieving a steady state condition. Hence, temperature around the weld line decreases while temperatures in the region away from the weld line increases. The temperature history is predicted at a distance of 10 mm from the weld centreline on the top surface of the plate and compared with the results obtained from thermocouples at the same point as shown in **Fig. 11**. The thermal data derived from the numerical analysis aligns well with the experimental findings. The non-linear decreasing behaviour of temperature is due to the local heating by the welding electrode and the non-linear variation of the material's thermal properties with temperature. This high accuracy of the thermal model achieved in this work signifies the entire capability of thermo-mechanical analysis to define practical problems.

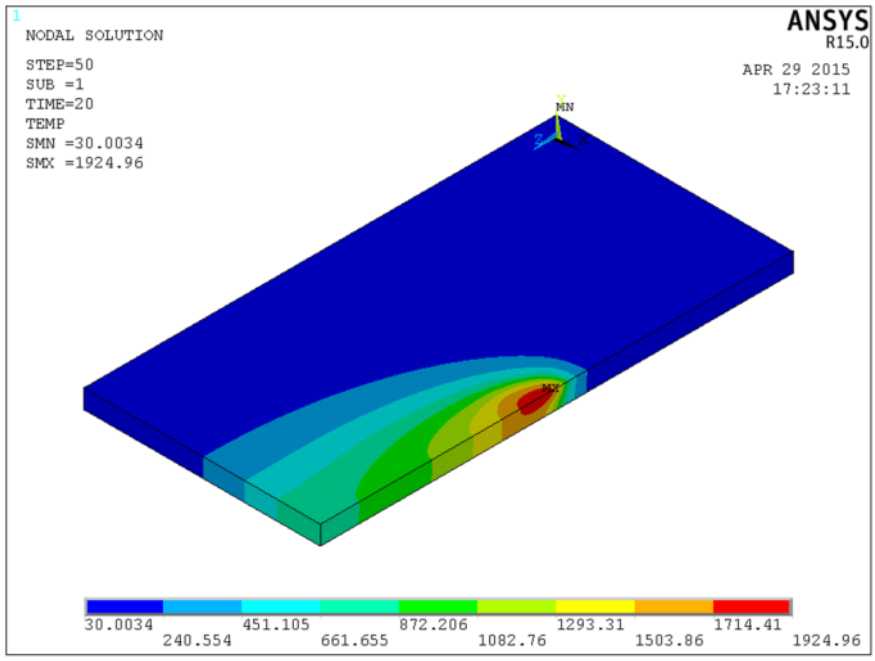

Fig. 9(a) : Temperature distribution at time = 20 seconds (middle position)

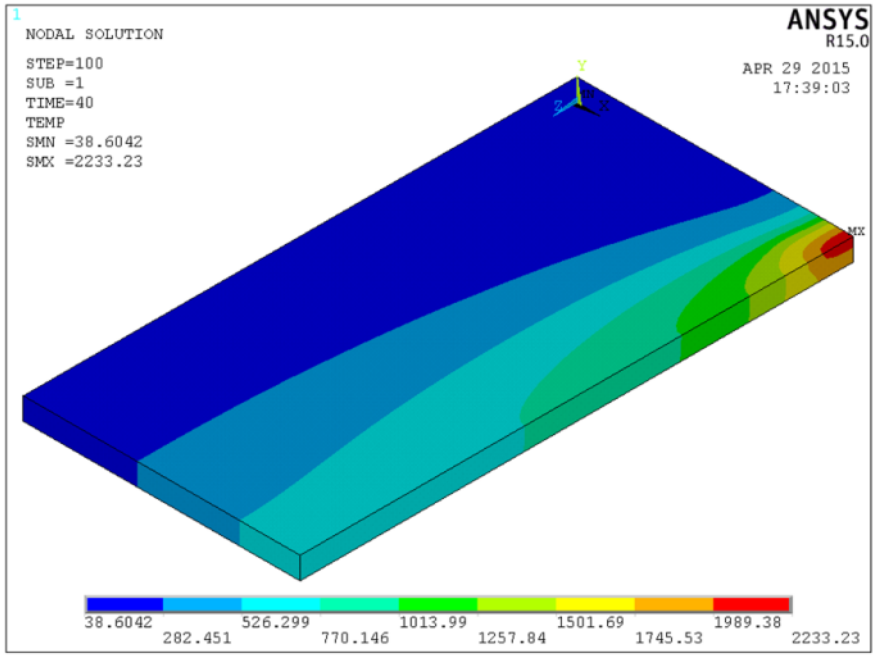

Fig. 9(b) : Temperature distribution at time = 40 seconds (weld stop position)

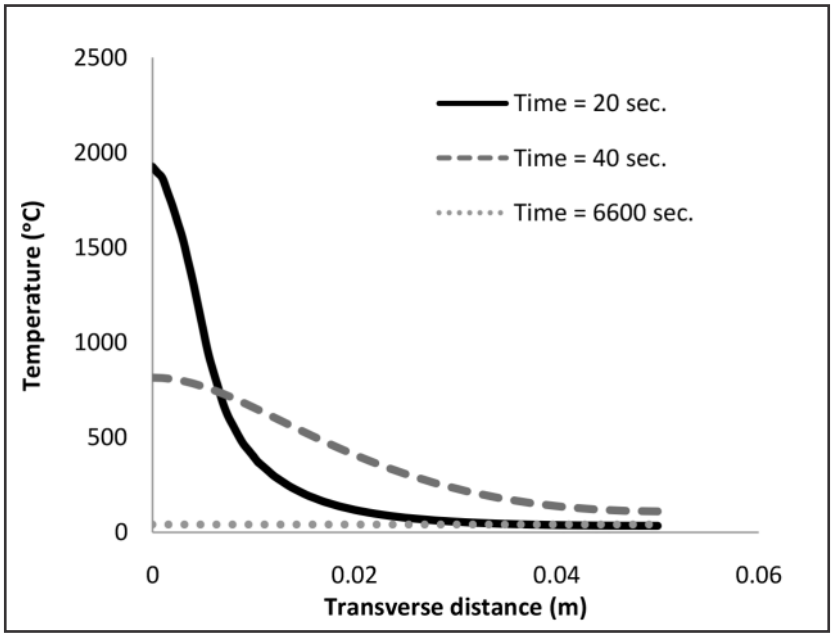

Fig. 10 : Temperature gradient along the transverse direction

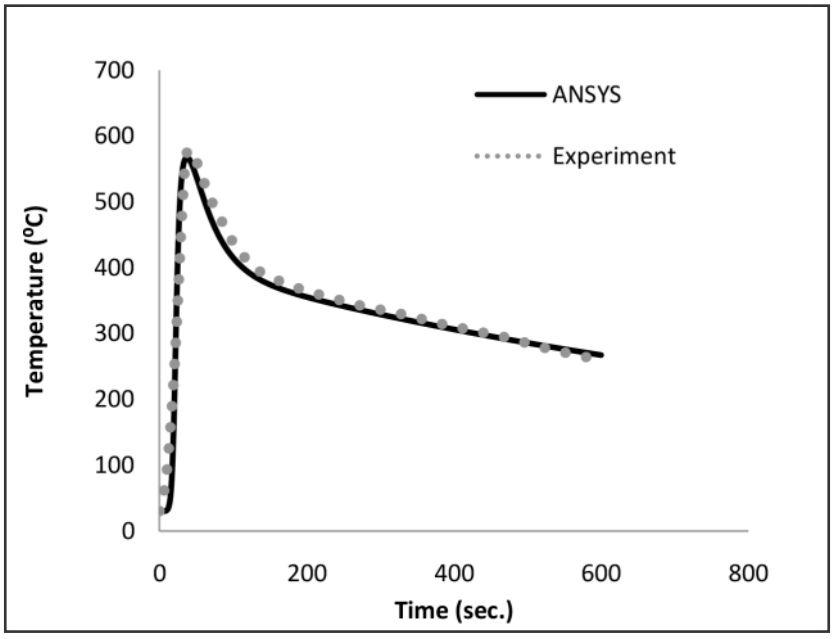

Fig. 11 : Temperature history at a point with distance 10 mm from weld centreline

4.2. Result of structural analysis

Fig.s 12 and **13** shows longitudinal stress distribution and transverse stress distribution on the top surface, at steady-state conditions. As the cooling process initiates, temperatures around the weld centreline area begin to decrease. Meanwhile, temperatures away from the weld centreline start rising due to heat conduction from the fusion zone. Thus, metal contracts close to the weld centreline and results in high tensile stress formation and also causes expansion of metal away from the weld centreline that results in compressive stress in that region. Longitudinal stress is plotted along transverse distance at mid-length of the plate as shown in **Fig. 14**, which exhibiting the progression of maximum tensile stress along the weld line, it subsequently diminishes to zero and eventually transforms into compressive stress with increased distance from the weld line. This kind of distribution is developed to maintain the self-equilibrium condition.

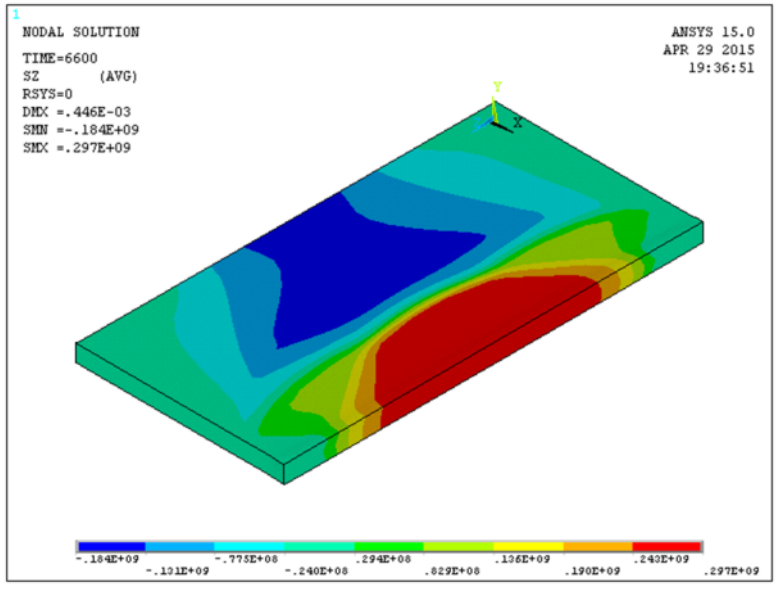

Fig. 12 : Longitudinal stress distribution at time = 6600 seconds

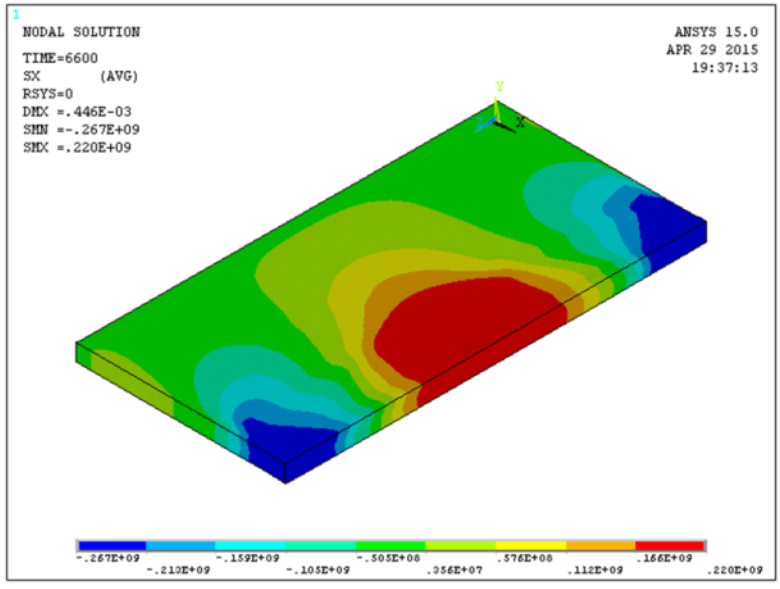

Fig. 13 : Transverse residual stress distribution at time = 6600 seconds

The observed maximum stresses align longitudinally and possess a magnitude nearly equivalent to the material's yield stress. It results due to a large amount of restrained thermal expansion and contraction in the middle of a weldment. **Fig. 15** represents transverse stress along the weld centreline at steady state condition. Maximum tensile stress in the transverse direction is found less than the maximum tensile stress in longitudinal direction. Maximum compressive stresses are formed at the weld toe having a magnitude greater than the maximum tensile stress. Angular distortion at the points on extreme edge of plate at mid length is measured using a simple method, and results are found to be very close to numerical data as shown in **Fig. 16**. The weld centreline is considered as datum line for measuring angular distortion and corresponding maximum distortion is found at the extreme edge of plate as the edges are not restrained with any external constraints. A comparison of numerical and experimental data shows that, the element modelling technique can be effectively used to estimate the temperature distributions, residual stresses, and distortions induced by the butt welding of two plates

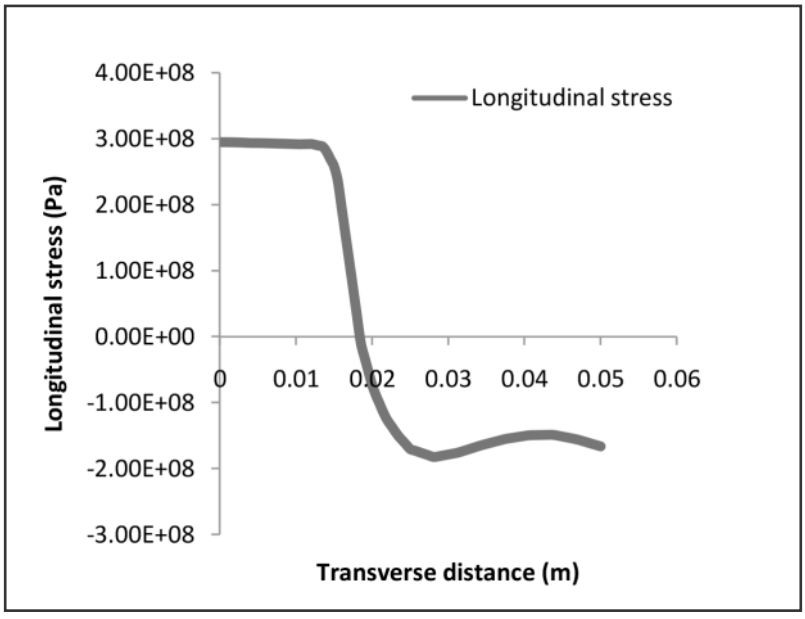

Fig. 14 : Longitudinal stress distribution along transverse distance

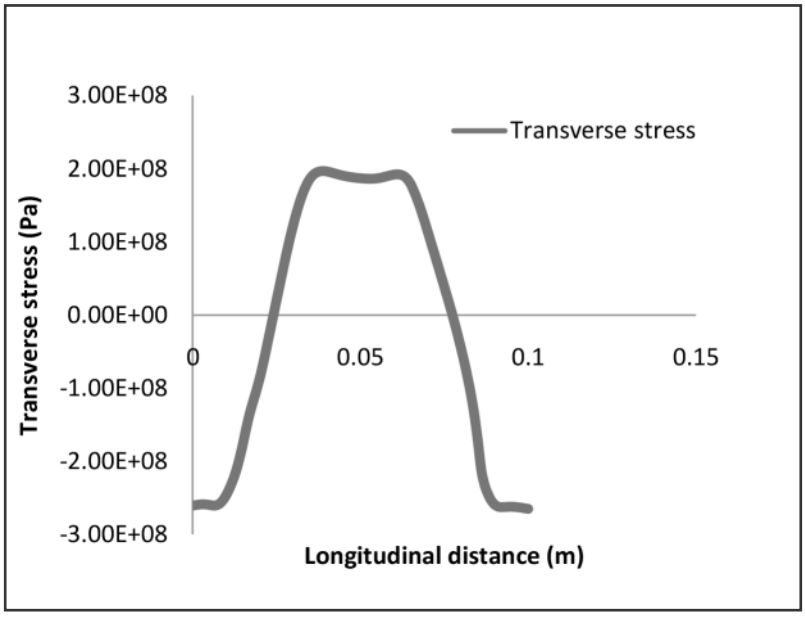

Fig. 15 : Transverse stress distribution along weld centreline

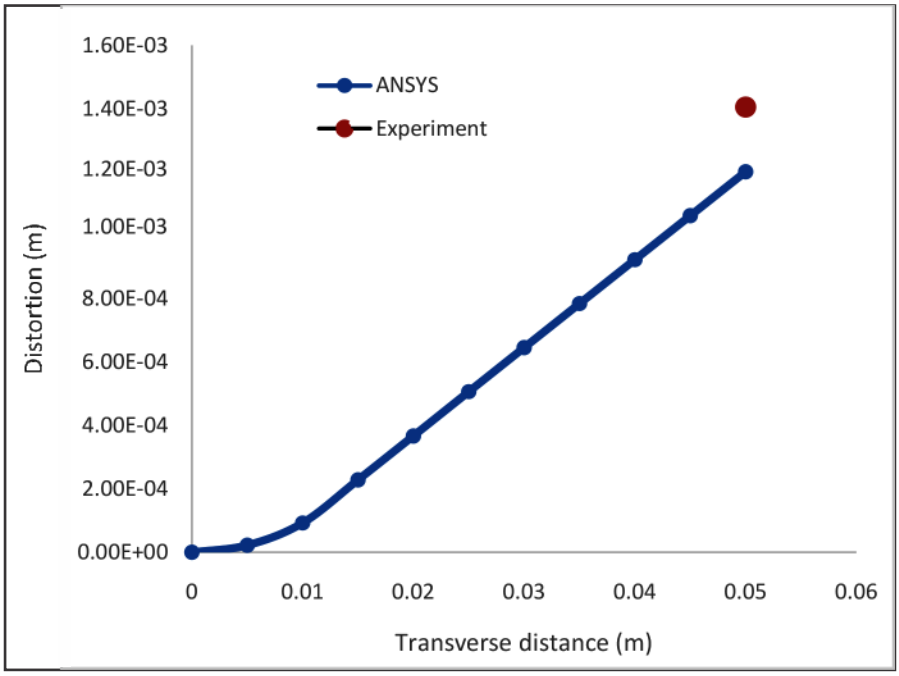

Fig. 16 : Distortion at mid-length of the plate

In order to strengthen the outcome of experimental work, the strength and hardness achieved in the welded joints are also checked. A tensile test of welded joint material is performed according to ASTM E8 on a universal testing machine and corresponding stress versus displacement plot is recorded. From the results of tension test, it is observed that the measured yield strength is 360 MPa, and the tensile strength is 540 MPa. Hence, the results of the tension test satisfy the specifications given in ASME Section Part II A.

Similarly, the hardness test of welded sample is also carried out using Vicker's cum Brinell hardness tester at different locations, i.e. at the weld zone, HAZ and parent metal according to ASTM E92. It is observed that the Vicker's hardness number decreases as the distance from the weld zone increases. Maximum hardness with magnitude 192 VHN is observed in the weld zone due to the difference in the microstructure of weld metal and parent metal. Furthermore, higher hardness is observed in the HAZ compared to parent metal due to its higher cooling rate and difference in microstructure. Measured hardness satisfies typical hardness values of SA516 Grade-70 carbon steel material. This confirms that necessary experiments are conducted as per requirements and results are realistic and hence can be compared directly with the simulated results. Thus, application of this approach will be helpful to the welding engineers to set the orientation and location of clamps during welding operation to overcome the predicted distortion.

5.0 CONCLUSIONS

Conducting a three-dimensional thermo-mechanical analysis of a SMAW process is vital to estimate transient temperature distribution, residual stress distribution, and distortion in the butt-welded SA516 Grade-70 steel. An experimental verification of thermal history and distortion had shown close agreement between the numerical and experimental data. Thus, numerical model can be used to estimate thermal and structural behaviour during the welding process. High-temperature gradient along transverse direction is found near the weld bead with a non-linear behaviour of temperature in decreasing order. A welding process also induces maximum longitudinal residual stress having nearly same order of magnitude as that of the yield stress of material. This type of approach is useful for the industries where welded components are very costly or requires high precision in the welded structure. Further, the residual stresses and distortion can also be minimized by predicting their magnitude and distributions through this approach and subsequently taking necessary precautions during the design stage.

REFERENCES

[1] Lindgren LE (2007); Computational welding mechanics, Woodhead Publishing, Cambridge.

[2] Attarha MJ and Sattari FI (2011); Study on welding temperature distribution in thin welded plates through experimental measurements and finite element simulation, Journal of Materials Processing Technology, 211(4), pp.688-694.

[3] Panwala MSM, Channiwala SA and Shrinivasan KN (2009); Numerical simulation of transient temperature in SMAW, Proceedings of the ASME 2009 Pressure Vessel and Piping Conference, Prague, Czech Republic, pp.449-456.

[4] do Carmo DA and de Faria AR (2015); A 2D finite element with through the thickness parabolic temperature distribution for heat transfer simulations including welding, Finite Elements in Analysis and Design, 93(1), pp.85-95.

[5] Mahapatra MM, Datta GL, Pradhan B and Mandal NR (2006); Three-dimensional finite element analysis to predict the effects of SAW process parameters on temperature distribution and angular distortions in single-pass butt joints with top and bottom reinforcements, International Journal of Pressure Vessels and Piping, 83(10), pp.721-729.

[6] Mollicone P, Camilleri D, Gray TG and Comlekci T (2006); Simple thermo-elastic–plastic models for welding distortion simulation, Journal of Materials Processing Technology, 176(1-3) pp.77-86.

[7] Goldak J, Chakravarti A and Bibby M (1984); A new finite-element model for welding heat-sources, Metallurgical Transaction B, 15(2), pp.299-305.

[8] Anca A, Cardona A, Risso J and Fachinotti VD (2011); Finite element modeling of welding processes, Applied Mathematical Modelling, 35(2), pp.688-707.

[9] Shan X, Davies CM, Wangsdan T, O'Dowd NP and Nikbin KM (2009); Thermo-mechanical modelling of a single-bead-on-plate weld using the finite element method, International Journal of Pressure Vessels and Piping, 86(1), pp.110-121.

[10] Slovacek M, Divis V, Junek L and Ochodek V (2005); Numerical simulation of the welding process - distortion and residual stress prediction, heat source model determination, Welding in the World, 49(11-12), pp.15-29.

[11] Barroso A, Canas J, Picon R, Paris F, Mendez C and Unanue I (2010); Prediction of welding residual stresses and displacements by simplified models. Experimental validation, Materials & Design, 31(3), pp.1338-1349.

[12] Jia X, Xu J, Liu Z, Huang S, Fan Y and Sun Z (2014); A new method to estimate heat source parameters in gas metal arc welding simulation process, Fusion Engineering and Design, 89(1), pp.40-48.

[13] Bhatti AA, Barsoum Z, Murakawa H and Barsoum I (2015); Influence of thermo-mechanical material properties of different steel grades on welding residual stresses and angular distortion, Materials & Design, 65(1), pp.878-889.

[14] Yadav A, Ghosh A and Kumar A (2017); Experimental and numerical study of thermal field and weld bead characteristics in submerged arc welded plate, Journal of Materials Processing Technology, 248(1), pp.262-274.

[15] Ghosh A, Chattopadhyaya S and Hloch S (2012); Prediction of weld bead parameters, transient temperature distribution and HAZ width of submerged arc welded structural steel plates, TehnickiVjesnik, 19(3), pp.617-620.

[16] Negi V and Chattopadhyaya S (2013); Critical assessment of temperature distribution in submerged arc welding process, Advances in Materials Science and Engineering, 2013(1), pp.1-9.

[17] Chang PH and Teng TL (2004); Numerical and experimental investigations on the residual stresses of the butt-welded joints, Computational Materials Science, 29(4), pp.511-522.

[18] Deng D and Murakawa H (2008); Prediction of welding distortion and residual stress in a thin plate butt-welded joint, Computational Materials Science, 43(2), pp.353-365.

[19] Zhu XK and Chao YJ (2002); Effect of temperature dependent material properties on welding simulation, Computers & Structures, 80(11), pp.967-976.

[20] Teng TL, Chan PH and Tseng WC (2003); Effect of welding sequences on residual stresses, Computers & Structures, 81(5), pp.273-286.

[21] Li C and Wang Y (2013); Three-dimensional finite element analysis of temperature and stress distributions for in-service welding process, Materials & Design, 52(1), pp.1052-1057.

[22] Islam M, Buijk A, Rais-Rohani M and Motoyama K (2014);Simulation-based numerical optimization of arc welding process for reduced distortion in welded structures,Finite Elements in Analysis and Design, 84(1), pp.54-64.

[23] Xia J and Jin H (2017); Numerical study of welding simulation and residual stress on butt welding of dissimilar thickness of austenitic stainless steel, The International Journal of Advanced Manufacturing Technology, 91(1-4), pp.227–235.

[24] Pu X, Zhang C, Li S and Deng D (2017); Simulating welding residual stress and deformation in a multi-pass butt-welded joint considering balance between computing time and prediction accuracy, The International Journal of Advanced Manufacturing Technology,93(5-8), pp.2215–2226.

[25] Wei L, Geng X and Du A (2018);Theoretical analysis and experimental study on heat transfer mechanism and thermal insulation properties of composite insulation coating, International Journal of Simulation and Process Modelling, 13(3), pp.272-280.

[26] Kalyankar VD and Pujari A (2018);Simulation and design optimisation of broach tool geometry for enhancing material removal rate, International Journal of Simulation and Process Modelling, 13(3), pp.264-271.

[27] Dar NU, Qureshi EM and Hammouda MMI (2009); Analysis of weld-induced residual stresses and distortions in thin-walled cylinders, Journal of Mechanical Science and Technology, 23(4), pp.1118-1131.

[28] Karlsson RI and Josefson BL (1990); Three-dimensional finite element analysis of temperature and stress in single-pass butt-welded pipe, Journal of Pressure Vessel Technology, 112(1), pp.76-84.

[29] Brown SB and Song H (1992); Implications of three-dimensional numerical simulations of welding of large structures, Welding Journal, 71(2), pp.55-62.